Syntaxin-binding protein STXBP5 inhibits endothelial exocytosis and promotes platelet secretion

Qiuyu Zhu,[1,2] Munekazu Yamakuchi,[1,3] Sara Ture,[1] Maria de la Luz Garcia-Hernandez,[1] Kyung Ae Ko,[1] Kristina L. Modjeski,[1,2] Michael B. LoMonaco,[1] Andrew D. Johnson,[4] Christopher J. O'Donnell,[4,5] Yoshimi Takai,[6] Craig N. Morrell,[1] and Charles J. Lowenstein[1]

[1]Aab Cardiovascular Research Institute, Department of Medicine, University of Rochester Medical Center, Rochester, New York, USA. [2]Department of Pharmacology and Physiology, University of Rochester School of Medicine and Dentistry, Rochester, New York, USA. [3]Department of Laboratory and Vascular Medicine, Kagoshima University Graduate School of Medicine and Dentistry, Kagoshima, Japan. [4]Division of Intramural Research, National Heart, Lung, and Blood Institute (NHLBI), NIH, and NHLBI's Framingham Heart Study, Framingham, Massachusetts, USA. [5]Cardiovascular Division, Massachusetts General Hospital, Harvard Medical School, Boston, Massachusetts, USA. [6]Department of Biochemistry and Molecular Biology, Kobe University Graduate School of Medicine, Kobe, Japan.

In humans, vWF levels predict the risk of myocardial infarction and thrombosis; however, the factors that influence vWF levels are not completely understood. Recent genome-wide association studies (GWAS) have identified syntaxin-binding protein 5 (*STXBP5*) as a candidate gene linked to changes in vWF plasma levels, though the functional relationship between *STXBP5* and vWF is unknown. We hypothesized that STXBP5 inhibits endothelial cell exocytosis. We found that STXBP5 is expressed in human endothelial cells and colocalizes with and interacts with syntaxin 4. In human endothelial cells reduction of STXBP5 increased exocytosis of vWF and P-selectin. Mice lacking *Stxbp5* had higher levels of vWF in the plasma, increased P-selectin translocation, and more platelet-endothelial interactions, which suggests that STXBP5 inhibits endothelial exocytosis. However, *Stxbp5* KO mice also displayed hemostasis defects, including prolonged tail bleeding times and impaired mesenteric arteriole and carotid artery thrombosis. Furthermore, platelets from *Stxbp5* KO mice had defects in platelet secretion and activation; thus, STXBP5 inhibits endothelial exocytosis but promotes platelet secretion. Our study reveals a vascular function for STXBP5, validates the functional relevance of a candidate gene identified by GWAS, and suggests that variation within *STXBP5* is a genetic risk for venous thromboembolic disease.

Introduction

Venous thromboembolism is a major cause of morbidity and mortality (1, 2). Venous thrombosis is the second leading cause of death in patients with cancer (3). The pathophysiology of venous thromboembolism includes abnormalities in blood flow, the vessel wall, and coagulation factors such as vWF (4, 5). Endothelial cells (ECs) lining the vessel wall maintain the integrity of the vasculature. Under normal conditions, ECs inhibit thrombosis by producing NO, prostacyclin, and other antithrombotic factors (6–9). When pathologic processes injure the vessel wall, ECs decrease production of antithrombotic factors and increase production of prothrombotic factors that play a critical role in initiating thrombus formation.

One of the earliest EC responses to injury is exocytosis (10). Various stimuli, including hypoxia, physical trauma, and inflammatory mediators, trigger ECs to release the contents of granules called Weibel-Palade bodies (WPBs) (11). vWF, a glycoprotein involved in hemostasis, is the major constituent released from WPBs. Released vWF initiates platelet adherence to the vessel by binding to platelet glycoproteins and to components of the extracellular matrix of the vessel wall (12). P-selectin externalized by endothelial exocytosis activates leukocyte rolling along the vessel lumen, the first step in leukocyte trafficking. Endothelial granules also contain additional proinflammatory and prothrombotic mediators that activate inflammation and thrombosis in response to vascular injury (10, 13). Together, these compounds trigger a cascade of events leading to thrombosis and inflammation (10, 14–16). Endothelial exocytosis is thus a novel therapeutic target for thrombotic diseases (17–19).

The exocytic machinery that drives vesicle trafficking and membrane fusion in ECs is similar to that found in neurons and yeast (20–24). Soluble *N*-ethylmaleimide–sensitive factor (NSF) attachment protein receptor (SNARE) molecules on the endothelial granule surface interact with specific SNAREs on the plasma membrane surface, forming a SNARE complex that bridges the 2 membranes and directs vesicle fusion with the plasma membrane (25, 26). Recent studies have defined some of the endothelial proteins that control vesicle secretory pathway in ECs. Syntaxins, vesicle-associated membrane proteins (VAMPs), synaptosomal-associated proteins (SNAPs), NSF, α-synuclein, and various small GTPases and their effectors (such as Rab11, RalA, Rap1, Rab27a, MyRIP, and Slp4-a) play a critical role in endothelial granule exocytosis (27–34); NO and thioredoxin regulate exocytosis by chemically modifying NSF (35, 36); and an assortment of secretagogues or pathologic stimuli can stimulate granule secretion from human

▶ Related Commentary: p. 4231

Conflict of interest: Yoshimi Takai serves on scientific advisory boards for, and has received consulting fees from, Kan Research Institute Inc. and Asubio Pharma Co.
Submitted: May 24, 2013; **Accepted:** July 24, 2014.
Reference information: *J Clin Invest*. 2014;124(10):4503–4516. doi:10.1172/JCI71245.

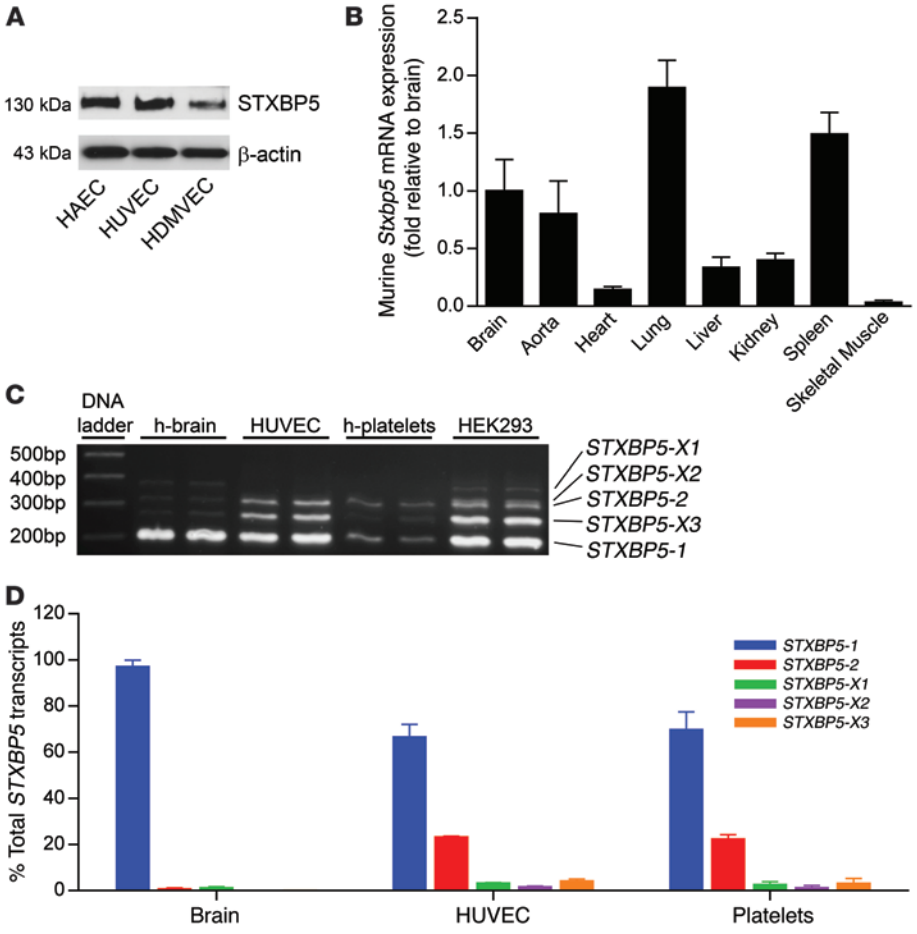

Figure 1. STXBP5 expression and transcript variants. (**A**) STXBP5 expression in human ECs. Lysates of cultured HAECs, HUVECs, and HDMVECs were probed by IB with antibody against STXBP5. Blotting to β-actin was used as a loading control. Representative of 3 separate experiments. (**B**) *Stxbp5* expression in murine tissue. RNA was isolated from WT mouse tissues, and *Stxbp5* mRNA expression was measured by qPCR and normalized to mRNA level in brain (n = 3). (**C**) Human *STXBP5* transcript variants. *STXBP5* transcript variants were detected by RT-PCR using primers flanking splice region in human brain, HUVECs, human platelets, and HEK293 cells. The products were separated by agarose gel, sequenced, and compared with NCBI reference sequences (*STXBP5-X1*, PCR product 370 bp in length, 99% similarity to NCBI entry; *STXBP5-X2*, 322 bp, 95% similarity; *STXBP5-2*, 307 bp, 100% similarity; *STXBP5-X3*, 262 bp, 100% similarity; *STXBP5-1*, 199 bp, 100% similarity). (**D**) Relative abundance of *STXBP5* transcript variants in human brain, HUVECs, and human platelets, measured by qPCR using variant-specific Taqman probes and expressed relative to brain *STXBP5-1* (assigned as 100%) (n = 3). All data are mean ± SD.

ECs through discrete signaling pathways (37–44). However, the detailed mechanisms controlling the endothelial SNARE machinery are not fully known.

Recently, genome-wide association studies (GWAS) identified novel genetic variants that are associated with altered plasma vWF levels in humans (45–47). These genetic loci might indicate novel genes whose products regulate endothelial exocytosis. The genetic locus with the highest significance is located within the gene syntaxin-binding protein 5 (*STXBP5*). This association was strikingly reaffirmed by studies on venous thrombosis in humans (48). The prominent relationship between human plasma vWF alterations and genetic variation of *STXBP5* prompted us to investigate the potential role of STXBP5 in endothelial exocytosis.

STXBP5 was first discovered as a protein interacting with syntaxin 1A (STX1) in neuron and named tomosyn (49). It is enriched in rat brain and is also found in the heart, spleen, lung, liver, skeletal muscle, kidney, and testis (49, 50). The *STXBP5* gene (originally known as *tomosyn*, later *tomosyn-1*) is located on mouse chromosome 10 and human chromosome 6. Murine *Stxbp5* has at least 3 transcript variants: *Stxbp5-b*, *Stxbp5-m*, and *Stxbp5-s*. Human *STXBP5* has at least 5 predicted transcript variants: *STXBP5-1*, *STXBP5-2*, *STXBP5-X1*, *STXBP5-X2*, and *STXBP5-X3*. The gene *Stxbp5L* (originally called *tomosyn-2*) is located on mouse chromosome 16 and human chromosome 3. Murine *Stxbp5L* has at least 4 transcript variants: *Stxbp5L-xb*, *Stxbp5L-b*, *Stxbp5L-m*, and *Stxbp5L-s* — all with distinct distribution patterns (50, 51). All STXBP5 isoforms possess an N-terminal domain that contains WD40 repeats and a C-terminal domain that includes an R-SNARE–like motif (50–52). The R-SNARE domain mediates the interaction of STXBP5 with STX1 and blocks formation of the heterotrimeric SNARE complex composed of STX1, VAMP2, and SNAP25 (53, 54). STXBP5 inhibits neuron release of neurotransmitters and endocrine cell secretion of insulin or other vesicles (55–61). However, the role of STXBP5 in the vasculature has never been studied, and the relation of STXBP5 with thrombosis has not been explored.

Here we showed that mammalian ECs express STXBP5. In vitro, STXBP5 interacted with the endothelial exocytic machinery and was a potent regulator of endothelial exocytosis. Using KO mice, we showed that STXBP5 regulated plasma vWF levels and platelet adhesion to the vessel wall. STXBP5 also regulated platelet secretion and thrombosis. These data suggest that STXBP5 is a novel regulator of endothelial exocytosis and thrombosis.

Results

We first defined the expression of STXBP5 in human cells and in murine tissue. We performed IB for STXBP5 on cultured human aortic ECs (HAECs), human umbilical vein ECs (HUVECs), and human dermal microvascular ECs (HDMVECs). STXBP5 was expressed as a 130-kDa protein in all 3 human EC types (Figure 1A and ref. 49). *Stxbp5* mRNA was expressed in murine tissues, including lung, spleen, and aorta, as measured by quantitative real-time PCR (qPCR; Figure 1B). *Stxbp5* mRNA was also found

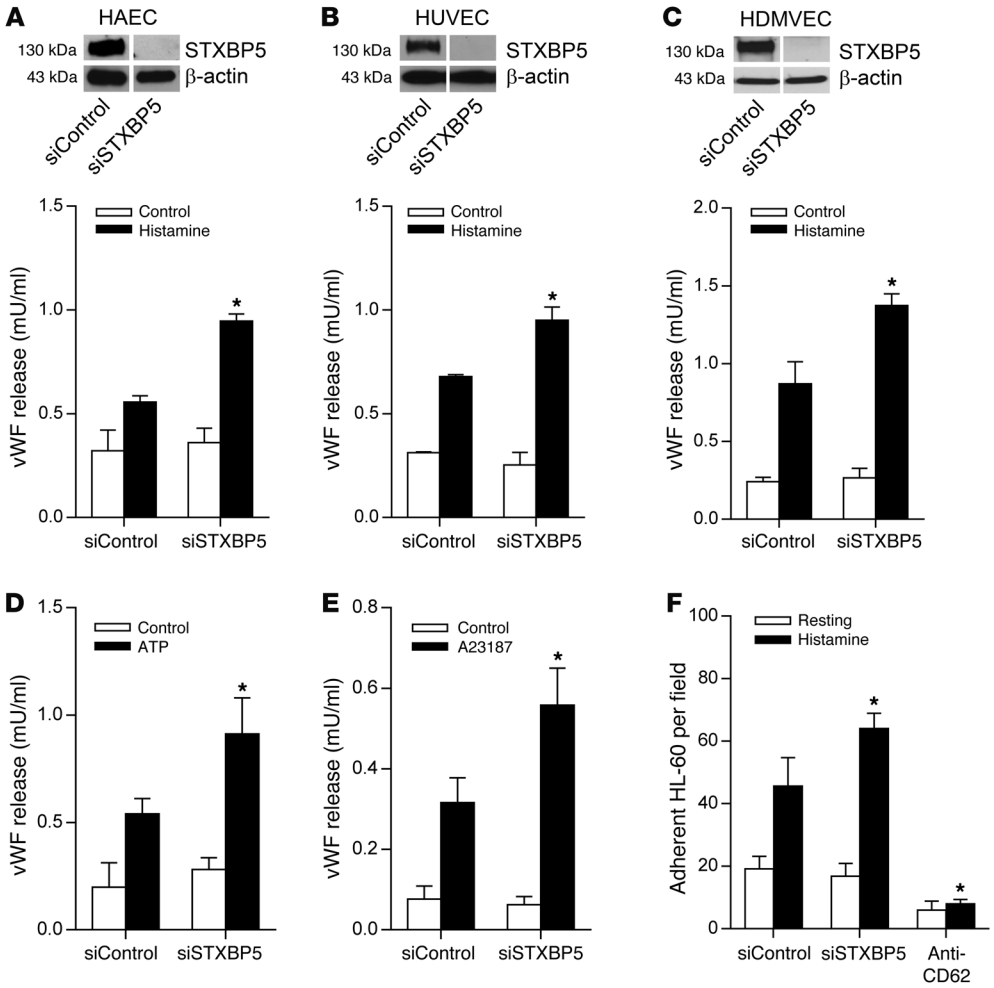

Figure 2. STXBP5 inhibits endothelial exocytosis in vitro. ECs were transfected with siRNA against STXBP5 (siSTXBP5) or control siRNA (siControl), stimulated with an agonist, and the amount of vWF released into the media at resting condition and after 30-minute stimulation was measured by ELISA (n = 3). (**A**–**C**) Knockdown of STXBP5 increased histamine-induced release of vWF, but had no effect on constitutive vWF release, in (**A**) HAECs, (**B**) HUVECs, and (**C**) HDMVECs. IB at top shows siRNA knockdown of STXBP5 expression in ECs, with endogenous actin as loading control. Lanes were run on the same gel but were noncontiguous. (**D** and **E**) Knockdown of STXBP5 in HUVECs increased vWF release induced by (**D**) ATP and (**E**) A23187. (**F**) Knockdown of STXBP5 in HUVECs increased P-selectin externalization, as measured by HL-60 cell adherence; cells treated with antibody against P-selectin (anti-CD62) served as a negative control. All data are mean ± SD. *$P < 0.05$ vs. siControl.

in murine brain, supporting studies identifying a role for *Stxbp5* in neurovesicle release (49, 54).

We next characterized the *STXBP5* isoforms expressed by human tissues and cells. We performed RT-PCR on RNA from HUVECs, human brain, human platelets, and HEK293 cells using primers flanking the splice regions. We identified 5 transcript variants of *STXBP5*, all of which have been predicted by computer algorithms, but not previously characterized: *STXBP5-1* (NM_139244.4), *STXBP5-2* (NM_001127715.2), *STXBP5-X1* (XR_245502.1), *STXBP5-X2* (XR_245503.1), and *STXBP5-X3* (XR_245504.1) (Figure 1C). To quantitate the relative abundance of each splice variant, we also performed qPCR. The *STXBP5* transcript variant expressed at highest levels by ECs was *STXBP5-1*, followed by *STXBP5-2*, and other transcript variants were expressed at lower levels (Figure 1D). However, whereas the *STXBP5* splice variant profile in platelets resembled that in ECs, human brain predominantly expressed *STXBP5-1*, and very little of the other variants (Figure 1D). Other studies confirm that the same isoform, *STXBP5-1*, is expressed in mammalian brain (49, 50).

We next explored the role of STXBP5 in endothelial exocytosis. We knocked down expression of endogenous STXBP5 by RNA interference in HAECs, HUVECs, and HDMVECs; stimulated the cells with the physiological agonist histamine; and then measured the amount of vWF released into the media using ELISA. siRNA directed against *STXBP5* decreased expression of STXBP5 in HAECs, HUVECs, and HDMVECs (Figure 2, A–C). Whereas knockdown of STXBP5 expression did not affect the constitutive secretion of vWF under resting conditions, it significantly increased histamine-induced vWF release into media in all 3 different EC types (Figure 2, A–C). Similarly, knockdown of STXBP5 in HUVECs increased vWF release induced by ATP and by the Ca^{2+} ionophore A23187, but did not change vWF release under the resting condition (Figure 2, D and E). We also explored the effect of STXBP5 upon externalization of P-selectin, another component of WPBs translocated by endothelial exocytosis (62). Knockdown of STXBP5 increased the endothelial externalization of P-selectin upon histamine stimulation, as measured by HL-60 cell adherence (Figure 2F and Supplemental Figure 1; supplemental material available online with this article; doi:10.1172/JCI71245DS1). To further characterize the effect of STXBP5 on constitutive release of vWF, we measured vWF levels in the media of HUVECs transfected with control siRNA or siRNA against STXBP5 over an extended period of 12 hours, and found no change in constitutive release (Supplemental Figure 2). STXBP5 did not affect total cellular vWF content (Supplemental Figure 3). We also tested the effect of genetic variation on STXBP5 function. We knocked down STXBP5 in ECs and then rescued STXBP5 expression with either WT STXBP5 or the N436S STXBP5 variant, which is associated with altered vWF levels in humans (47). N436S STXBP5 inhibited vWF secretion more effectively than did WT STXBP5 (Supplemen-

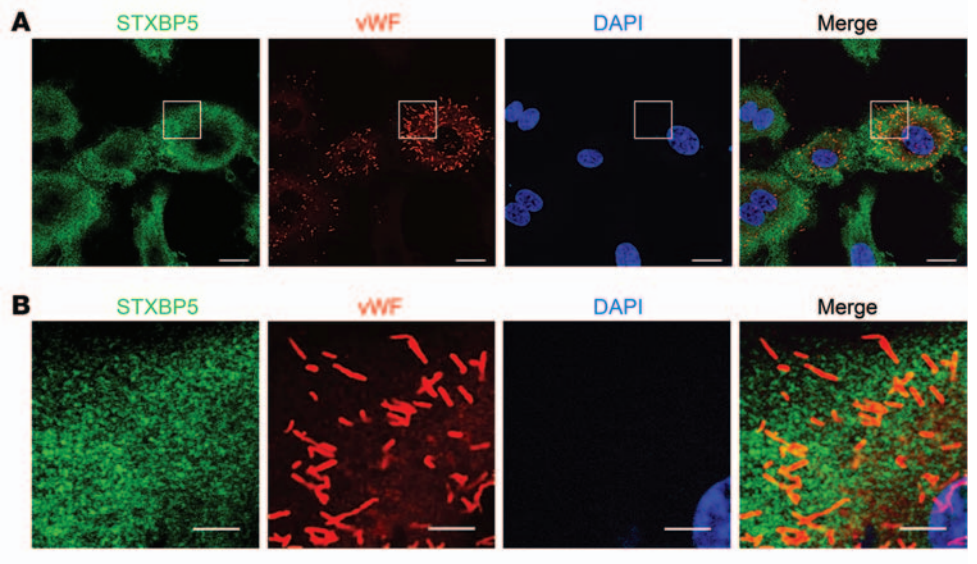

Figure 3. Particles containing STXBP5 are not colocalized with endothelial granules containing vWF. (**A**) HUVECs were imaged by confocal microscopy after staining with antibodies against STXBP5 (green), vWF (red), and DNA (DAPI; blue) (objective, oil ×40; confocal *z* resolution, 0.40 μm). (**B**) Enlargement of boxed regions in **A** (objective, oil ×40; confocal *z* resolution, 0.40 μm). STXBP5 was minimally colocalized with WPBs. Representative of more than 3 separate experiments. Scale bars: 20 μm (**A**); 5 μm (**B**).

tal Figure 4). Taken together, these results suggest that STXBP5 inhibits endothelial exocytosis.

We also tested the idea that STXBP5 affects vWF release by regulating granule number and morphology. We counted the number of WPB granules in HUVECs transfected with control or STXBP5 siRNA and found that STXBP5 did not affect WBP numbers per cell (Supplemental Figure 5). Analysis of individual WPBs revealed that STXBP5 did not affect the size of these granules (Supplemental Figure 6). Finally, we measured the morphology of WPBs by quantifying the aspect ratio of individual WPB granules, and found that STXBP5 did not affect this distribution (Supplemental Figure 7).

Since genetic variants in *STXBP5* are associated with alterations in vWF levels, we next defined the subcellular location of STXBP5 in relation to endothelial granules, which contain vWF as well as other proinflammatory and prothrombotic mediators. We found that STXBP5 was located in the cytoplasm, primarily in a punctate pattern (Figure 3). Immunostaining for vWF revealed the typical rod-shaped morphology of WPBs (Figure 3 and Supplemental Figure 7). Using confocal microscopy, we found that STXBP5 was minimally colocalized with vWF (Figure 3). The morphology of the particles containing STXBP5 was different from that of WPB granules containing vWF, and the overlap was minor (Figure 3). We searched for subcellular location of STXBP5: confocal microscopy did not reveal definitive colocalization with markers for the ER, Golgi, lysosome, or endosome compartments (Supplemental Figure 8).

We next searched for links between STXBP5 and the exocytic machinery in ECs. Prior studies showed that STXBP5 can inhibit neurotransmitter release from neurons and insulin release from pancreatic β cells by forming complexes with the SNARE proteins, including syntaxin isoforms and SNAP isoforms (49, 63–65). We and others have previously shown that SNARE molecules — including STX4, VAMP3, VAMP8, and SNAP23 — are involved in WPB exocytosis in ECs and play a pivotal role in this molecular machinery (27, 35, 66, 67). Accordingly, we searched for an interaction between STXBP5 and endothelial SNARE molecules. We first used sucrose density gradient ultracentrifugation to specify the cellular components that cosediment with STXBP5. We loaded HUVEC lysates on top of a 5%–40% discontinuous sucrose density gradient, performed ultracentrifugation, and analyzed fractions by IB. STXBP5 and STX4 partially cosedimented (Figure 4A), which suggests these 2 proteins might be able to form a complex in HUVECs and might interact directly or indirectly with each other. However, STXBP5 did not cosediment with other SNAREs involved in endothelial exocytosis, such as SNAP23 (Figure 4A).

To further characterize the interaction between STXBP5 and STX4, we immunoprecipitated HUVEC lysates with antibody against STXBP5 and subjected the precipitants to IB with antibody against STX4. STXBP5 coprecipitated with STX4, but not with STX11 or SNAP23 (Figure 4B).

We then searched for colocalization of STXBP5 and STX4 by immunofluorescence staining of HUVECs. STXBP5 and STX4 were both distributed in a punctate pattern, and a subset of STXBP5 colocalized with STX4 (Pearson coefficient, 0.80 ± 0.03; Figure 4C). Taken together, these data show that STXBP5 interacts with a complex containing STX4 in ECs. Given the pivotal role that STX4 plays in endothelial vesicle trafficking (35, 66), their interaction may underline the inhibitory function of STXBP5 in endothelial exocytosis.

We also searched for an association between STXBP5 and synaptotagmin 1 (SYT1). STXBP5 and SYT1 partially cosedimented and also coprecipitated, especially in cells stimulated with histamine or A23187 (Figure 4, A and B). We also searched for colocalization of STXBP5 and SYT1 by immunofluorescence staining of HUVECs. In resting HUVECs, STXBP5 and SYT1 were both distributed in a punctate pattern, and a subset of STXBP5 colocalized with SYT1 (Pearson coefficient, 0.70 ± 0.08; Figure 4D). Furthermore, both STXBP5 and SYT1 colocalized to plasma membranes of HUVECs after stimulation (Pearson coefficient, 0.69 ± 0.08; Figure 4D). These data reinforced prior observations that STXBP5 interacts with SYT1 in neurons (49, 68).

We also searched for interactions of STXBP5 and other molecules that regulate vesicle trafficking in ECs. STXBP5 did not coprecipitate with STX11, SNAP23, NSF, Munc18-2, or Munc18-3 (Figure 4B and Supplemental Figure 9). Furthermore, STXBP5 failed to colocalize significantly with other SNARE molecules, such as

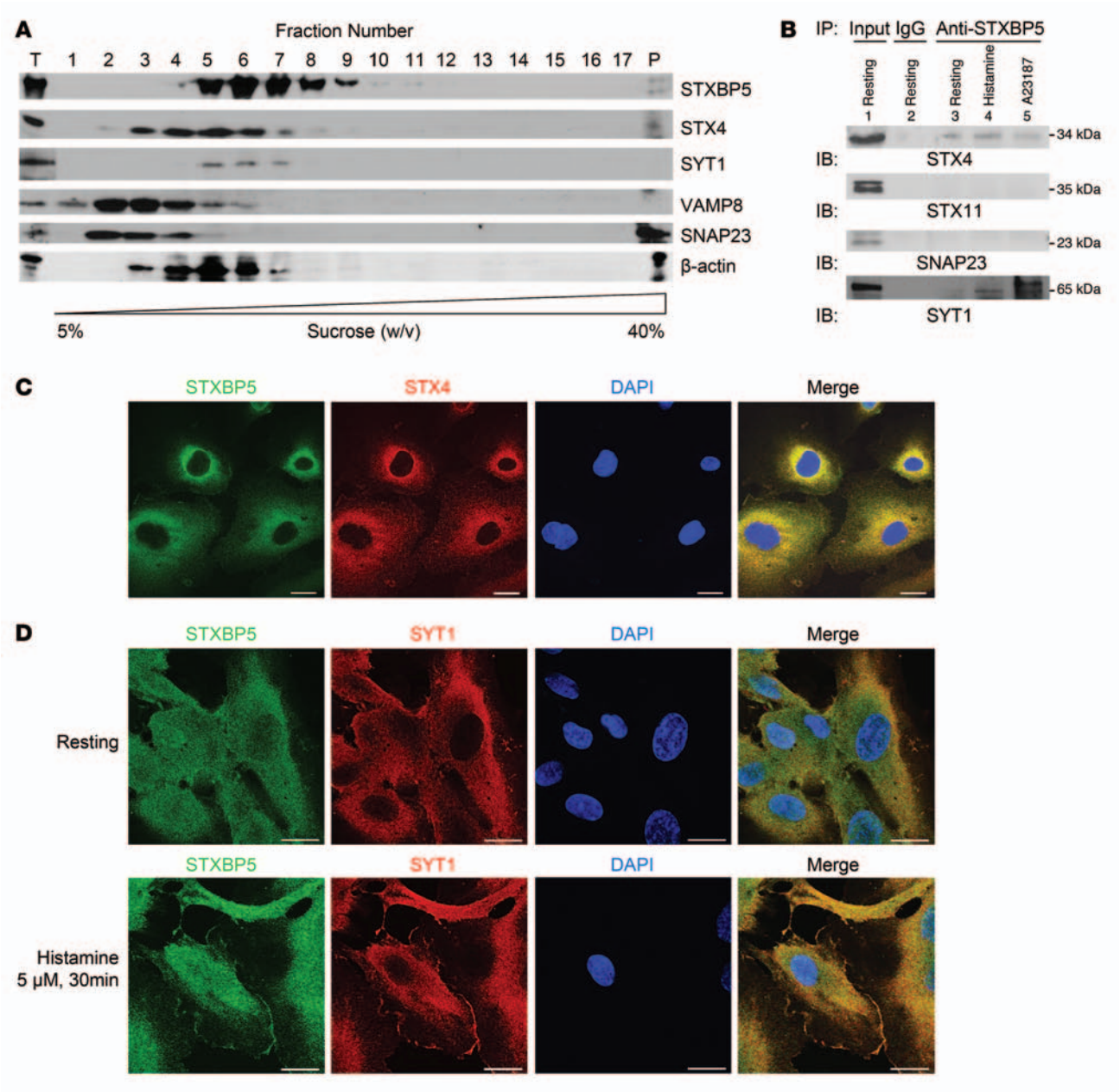

Figure 4. STXBP5 cosediments, colocalizes, and coprecipitates with STX4 and SYT1. (**A**) STXBP5 cosedimented with STX4 and SYT1 by sucrose density gradient fractionation. HUVEC lysate was ultracentrifuged through discontinuous 5%–40% sucrose gradient, and the fractions were analyzed by SDS-PAGE. T, total proteins of the lysate before fractionation; P, pellet after fractionation. Representative of 3 separate experiments. (**B**) STXBP5 coprecipitated with STX4 and SYT1. HUVEC lysate treated with media (resting), histamine, or A23187 was immunoprecipitated with antibody against STXBP5 or mouse IgG_1; precipitants were probed with antibody against SYT1, STX4, STX11, or SNAP23. Representative of 3 similar experiments. (**C**) STXBP5 colocalized with STX4 by confocal microscopy. HUVECs were stained for STXBP5 (green), STX4 (red), and DNA (DAPI; blue) (objective, oil ×40; confocal *z* resolution, 0.40 μm). STXBP5 partially colocalized with STX4. Pearson coefficient (green vs. red) was 0.80 ± 0.03. (**D**) STXBP5 colocalized with SYT1. Resting and stimulated HUVECs were stained for STXBP5 (green), SYT1 (red), and DNA (DAPI; blue) (objective, oil ×60; confocal *z* resolution, 0.32 μm). STXBP5 partially colocalized with SYT1, and both STXBP5 and SYT1 partially translocated to the membrane after stimulation. Pearson coefficient (green vs. red) was 0.70 ± 0.08 for resting cells, 0.69 ± 0.08 for histamine-stimulated cells. Scale bars: 20 μm.

SNAP23, VAMP8, and VAMP3 (Supplemental Figure 10). STXBP5 also did not colocalize with caveolin 1, Munc18-2, Munc18-3, NSF, Rab27a, Myosin 5a, or MyRIP (Supplemental Figures 11 and 12).

Taken together, our data suggest that STXBP5 interacts with a complex containing STX4 and SYT1 in ECs.

In order to test whether STXBP5 regulates endothelial exocytosis in vivo, we compared plasma levels of vWF in *Stxbp5*-deficient (*Stxbp5* KO) and WT mice. vWF levels were higher in *Stxbp5* KO than WT mice (Figure 5A), in agreement with our in vitro data showing greater vWF release from ECs with knockdown of STXBP5 than from control ECs (Figure 2). This difference in vWF levels was not due to the ADAMTS13 enzyme (which cleaves vWF in the blood), as ADAMTS13 activity was unchanged between WT and *Stxbp5* KO mice (Figure 5B).

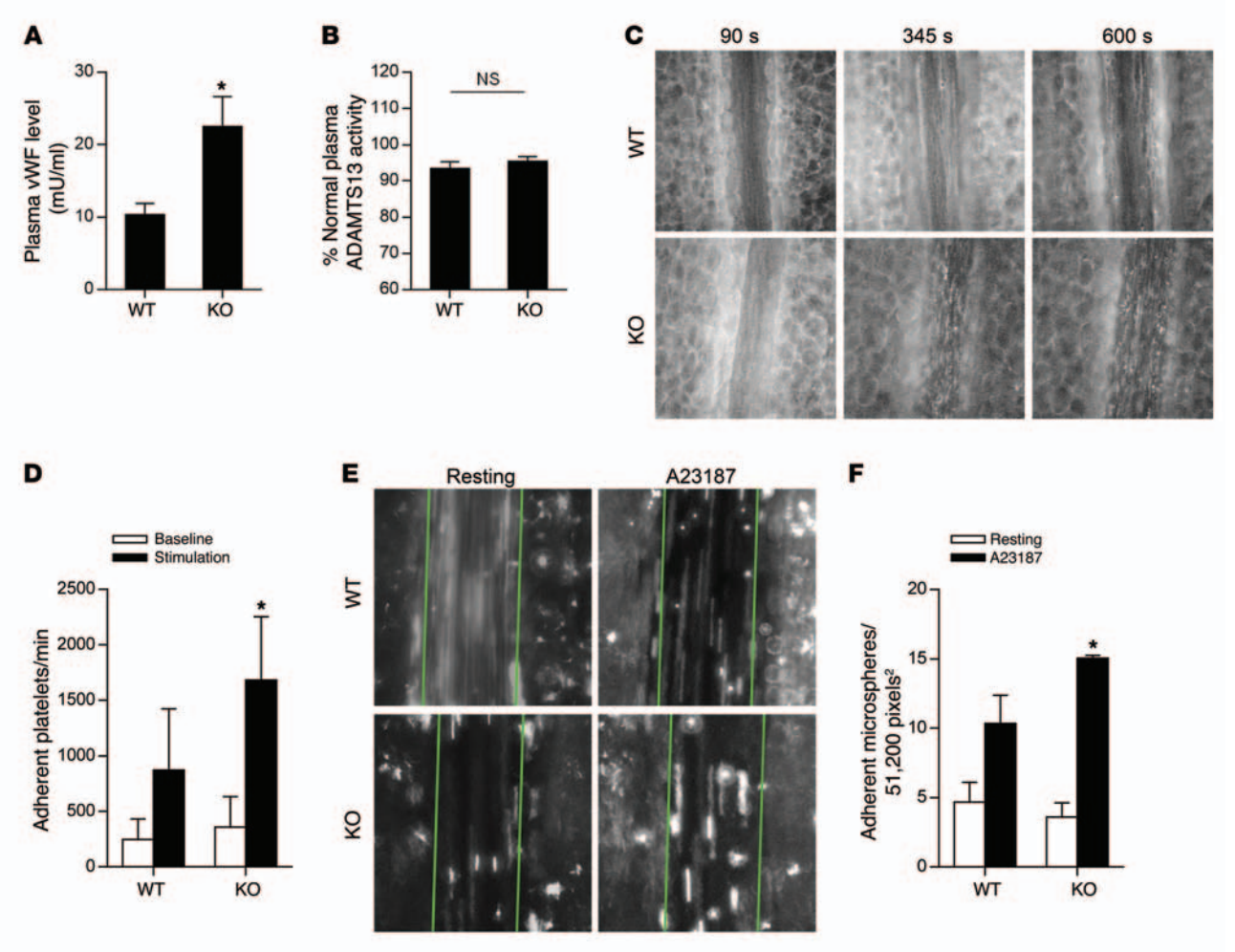

Figure 5. STXBP5 inhibits endothelial exocytosis in mice. (**A**) Higher plasma levels of vWF in *Stxbp5* KO than WT mice. Plasma vWF levels were measured by an ELISA from retroorbital bleeding (n = 8–12). (**B**) Similar plasma ADAMTS13 activity in *Stxbp5* KO and WT mice. ADAMTS13 activity in mouse plasma was measured by a fluorescent assay and expressed as percentage of that in pooled WT plasma. (**C**) Intravital microscopy of platelet-EC interactions in vivo. Platelets were fluorescently labeled in WT and *Stxbp5* KO mice. 10 μM A23187 was superfused onto the mesenteric venule after 120-second baseline recording. Platelet adhesion to the mesenteric venule was continuously recorded by intravital microscopy. Shown are representative images at baseline (90 seconds) and after A23187 stimulation (345 and 600 seconds). Original magnification, ×20. (**D**) *Stxbp5* deficiency increases platelet-EC interactions in vivo. Quantification of platelet adhesion in **C**, calculated by averaging the number of platelets that remained transiently within at least 2 consecutive frames, and expressed as adherent platelets per minute in a 51,200-pixel^2 area (n = 6 mice per genotype). (**E**) *Stxbp5* deficiency increases microsphere-EC interactions in vivo. Mice were perfused with fluorescent microspheres conjugated with antibody against P-selectin, and adhesion of microspheres was imaged 2 minutes before (resting) and 8 minutes after A23187 superfusion on mesenteric venule. Green lines denote the borders of the vessel within which adherent microspheres were counted. Original magnification, ×20. (**F**) Quantification of adherent microspheres in **E** (n = 3–4 mice per genotype). All data are mean ± SD. *P < 0.05 vs. WT.

To explore the physiological relevance of STXBP5, we measured the effect of STXBP5 upon platelet interactions with ECs in vivo. Platelet rolling or adherence to the vessel walls is mediated by vWF released by exocytosis (69). We hypothesized that deficiency of STXBP5 would permit an increase in WPB exocytosis, resulting in increased platelet adherence to venule walls. Anesthetized *Stxbp5* KO and WT mice were transfused with fluorescent antibodies to label platelets. The mesentery was externalized and superfused with 10 μM A23187 to stimulate WPB exocytosis, and intravital microscopy was used to record interactions of fluorescently labeled platelets with mesenteric venules. Platelets that remained static or were transiently captured by the endothelium and then released in a stop-and-go fashion in consecutive frames were considered adherent.

A23187 rapidly induced platelet adhesion to the venule wall in WT mice; in *Stxbp5* KO mice, A23187-induced platelet interaction with the venule wall was markedly increased (Figure 5C). Quantification of adherent platelets showed that STXBP5 deficiency significantly increased A23187-induced platelet interactions with the venule walls, but not the interaction in the resting condition (Figure 5D). This increase in platelet adherence to the venule is consistent with the notion of STXBP5 deficiency leading to increased exocytosis of WPBs and greater release of vWF.

Finally, we used an assay that directly measures endothelial exocytosis in order to eliminate the possible effects of STXBP5 on platelets. Mice were perfused with fluorescently labeled microspheres conjugated with antibody against P-selectin, and adhesion to resting and A23187-stimulated mesenteric venules was

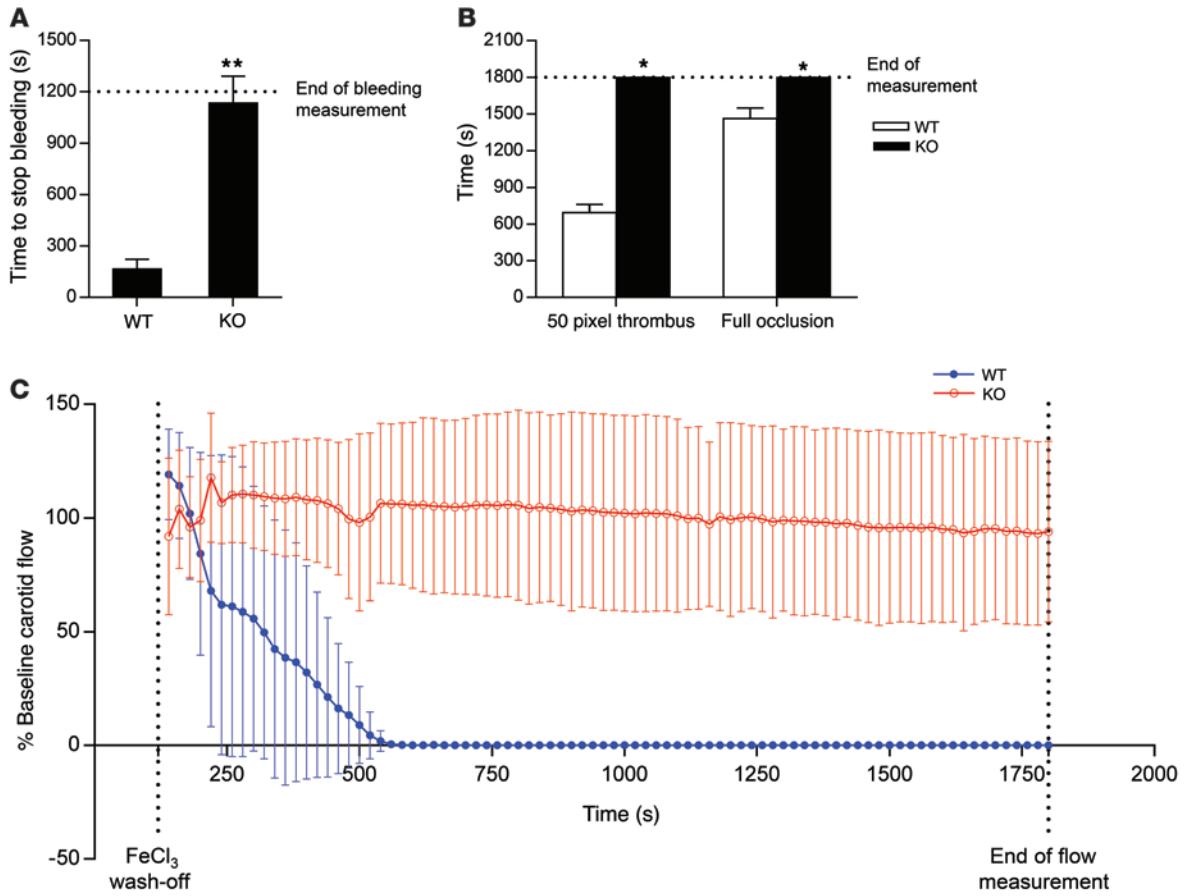

Figure 6. STXBP5 increases thrombosis in mice. (**A**) STXBP5 regulated bleeding time. Tail bleeding times in WT and *Stxbp5* KO mice were measured after distal 5-mm tail amputation (n = 10–12). (**B**) *Stxbp5* regulated mesenteric thrombosis. Intravital microscopy was used to measure thrombosis of mesenteric arterioles in WT and *Stxbp5* KO mice, including the time to form (left) a 50-pixel diameter thrombus and (right) full occlusion (n = 3–6). (**C**) STXBP5 regulated carotid thrombosis. Carotid arterial flow was measured (ml/min) by a Doppler flow probe after $FeCl_3$ injury, and flow after $FeCl_3$ wash-off was plotted as percentage of baseline flow before injury (n = 7). *Stxbp5* KO mice failed to form vessel occlusion. All data are mean ± SD. *$P < 0.05$, **$P < 0.01$ vs. WT.

imaged by intravital microscopy. A23187 treatment increased microsphere adherence to venules in WT mice, but the increase was even more in *Stxbp5* KO mice (Figure 5, E and F). This suggests that STXBP5 limits endothelial display of P-selectin in vivo. Taken together, these data show that STXBP5 inhibits endothelial exocytosis in vivo.

We proceeded to test the effect of STXBP5 on thrombosis. We expected that *Stxbp5* KO mice would have increased thrombosis, since they exhibited increased plasma vWF levels and platelet-endothelium interaction upon stimulation. We first measured the time for hemostasis in a murine tail bleeding model. Contrary to our expectations, *Stxbp5* KO mice displayed prolonged bleeding compared with WT mice (Figure 6A). We next measured the time for thrombosis in a murine mesenteric thrombosis model. *Stxbp5* KO mice had severely delayed time to formation of thrombus and time to vessel occlusion compared with WT mice (Figure 6B). We then measured the time for flow cessation in a murine carotid artery thrombosis model. Carotid artery flow ceased approximately 8 minutes after arterial injury in WT mice, compared with more than 30 minutes for *Stxbp5* KO mice (Figure 6C). Taken together, these data suggest that mice lacking STXBP5 have a defect in thrombosis.

These results were surprising: *Stxbp5* KO mice had elevated plasma levels of vWF, increased endothelial exocytosis, and increased platelet rolling along the vessel wall — but also had decreased thrombosis. One explanation for this apparent paradox is that STXBP5 also regulates platelet secretion.

To test the hypothesis that STXBP5 promotes platelet secretion, we first demonstrated that murine platelets expressed STXBP5 protein (Figure 7A). These data were consistent with our findings that human platelets expressed mRNA for *STXBP5* isoforms (Figure 1, C and D). We then explored the role of STXBP5 in platelet activation and secretion using platelets from WT and *Stxbp5* KO mice. To study platelet exocytosis of α granules, we measured externalization of P-selectin by flow cytometry. To study platelet secretion of dense granules, we measured release of ATP by a luciferase-based assay. To study platelet activation, we measured activation of the integrin GPIIbIIIα by flow cytometry. Platelets from *Stxbp5* KO mice showed defective P-selectin externalization, ATP release, and GPIIbIIIα activation (Figure 7B), which suggests that STXBP5 facilitates platelet exocytosis and activation.

To confirm these data, we analyzed WT mice that had received BM transplantation from WT or *Stxbp5* KO donors. Plasma levels of vWF were not changed by transplantation of WT or *Stxbp5* KO

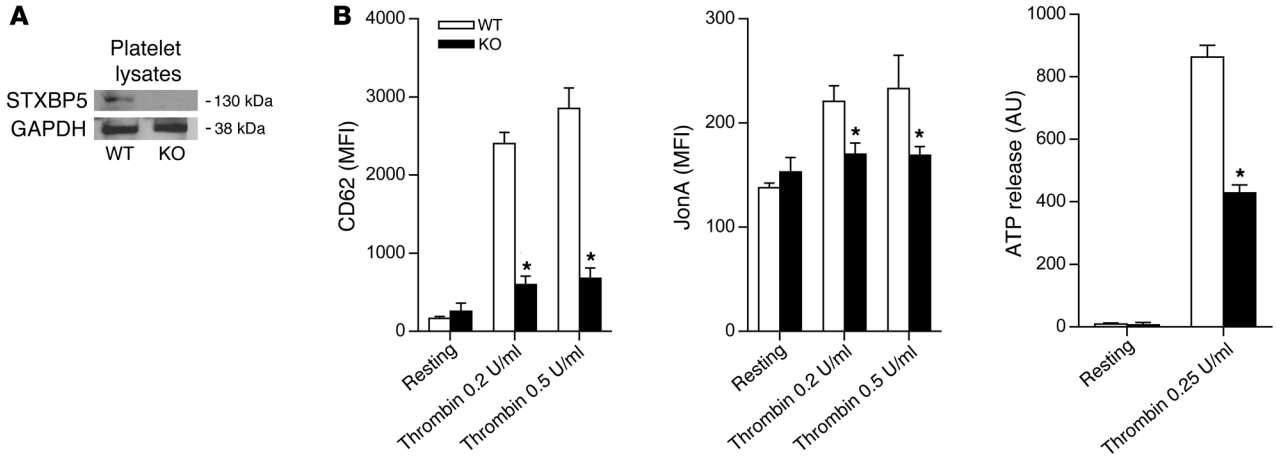

Figure 7. STXBP5 regulates platelet secretion and activation. (**A**) STXBP5 expression in platelets from WT and *Stxbp5* KO mice, determined by IB. GAPDH served as a loading control. (**B**) STXBP5 promoted platelet secretion. Platelets were isolated from WT and *Stxbp5* KO mice and stimulated with PBS (resting) or the indicated concentrations of thrombin. Median fluorescence intensity (MFI) changes were measured by flow cytometry after P-selectin externalization or integrin GPIIbIIIα activation (measured by CD62 and JonA fluorescence, respectively), and bioluminescence change was measured after ATP release (n = 3 per treatment). All data are mean ± SD. *$P < 0.05$ vs. WT.

donor BM; However, bleeding times were increased in the *Stxbp5* KO BM recipient mice (Figure 8, A and B). Furthermore, *Stxbp5* KO BM recipients failed to form an occlusive thrombus in a carotid artery thrombosis model (Figure 8C). Taken together, these data indicate that the thrombosis phenotype is determined by the BM cells (such as platelets), not by the host cells (such as ECs).

Discussion

The major finding of our study is that STXBP5 regulates endothelial and platelet exocytosis. STXBP5 interacted with components of the exocytic machinery and inhibited release of vWF in ECs and in mice. STXBP5 also promoted platelet secretion and thrombosis in mice. Thus, our present data provide strong functional evidence for the regulatory role on circulating vWF and thrombosis by a candidate gene previously identified by GWAS (45–48, 70).

We found that STXBP5 inhibited endothelial exocytosis. Others have found that STXBP5 inhibits secretion from other cell types. STXBP5 was originally identified as a protein that inhibits neurotransmitter release from neurons (49). Subsequent studies showed that STXBP5 decreases exocytosis in yeast, *C. elegans* synapses, pancreatic β cells, and neurosecretory cells (53, 55–61). We found that STXBP5 inhibited endothelial exocytosis of granules. Cells with decreased STXBP5 had increased vWF release into the media and increased display of P-selectin, and *Stxbp5* KO mice had elevated plasma vWF levels and greater display of P-selectin (Figures 2 and 5).

STXBP5 might regulate endothelial exocytosis through several potential mechanisms. One proposed model is that STXBP5 blocks formation of a ternary SNARE complex by competing with VAMP isoforms to interact with SNAP and syntaxin isoforms. For example, in neurons, the VAMP-like domain in the C terminus of STXBP5 forms a SNARE complex–like structure with SNAP25 and STX1. This STXBP5/SNARE complex is stable: VAMP2 cannot displace STXBP5, resulting in inhibition of SNARE complex assembly (52–54, 71). Alternatively, another proposal is that STXBP5 enhances oligomerization of the ternary SNARE complexes, locking them into a structure that cannot proceed with membrane fusion. For example, in neurons, the N-terminal WD40 repeat domain of STXBP5 functions as a scaffold that enhances oligomerization of preassembled SNARE complexes and reduces vesicle priming and turnover (56). In addition to these STXBP5/SNARE interaction models, *Sro7*, the yeast *STXBP5* homolog, acts as an allosteric regulator of exocytosis. The tail domain of Sro7 interacts with the Rab GTPase Sec4, raising the possibility that STXBP5 might be able to interact with some other factors that control exocytosis (72, 73). Our observation that STXBP5 interacted with a complex containing STX4 (Figure 4) favors the STXBP5/SNARE interaction model. STX4 is a target membrane SNARE (t-SNARE) that binds to cognate vesicle SNAREs (v-SNARE). The inhibition of vWF exocytosis is probably a consequence of displacement of the endothelial v-SNARE by STXBP5, forming a "dead-end" complex and sequestering the formation of productive SNARE complexes.

Another possible mechanism for STXBP5 inhibition of exocytosis is through its interaction with a calcium sensor, SYT1. SYT1 regulates SNARE-mediated vesicle fusion by bridging membrane fusion through a calcium-dependent mechanism (74–77). SYT1 has been shown to be recruited to pseudogranules containing heterologously expressed vWF (78). Others have demonstrated that STXBP5 interacts with SYT1 through a WD40 repeat domain in the N terminus of STXBP5, blocking the ability of SYT1 to mediate calcium-dependent neurotransmitter release (68). We also found that STXBP5 interacted with SYT1 more strongly after stimulation (Figure 4), which raises the possibility that calcium triggers exocytosis in part by relieving the inhibitory effects of STXBP5, either by displacing STXBP5 from t-SNAREs or by promoting interaction between STXBP5 and SYT1.

Our data raise some interesting issues. First, they suggest that STXBP5 inhibits secretory, but not constitutive, release of vWF (Figure 2). Recent studies suggest that ECs release vWF through 3 distinct pathways: stimulated secretion, unstimulated

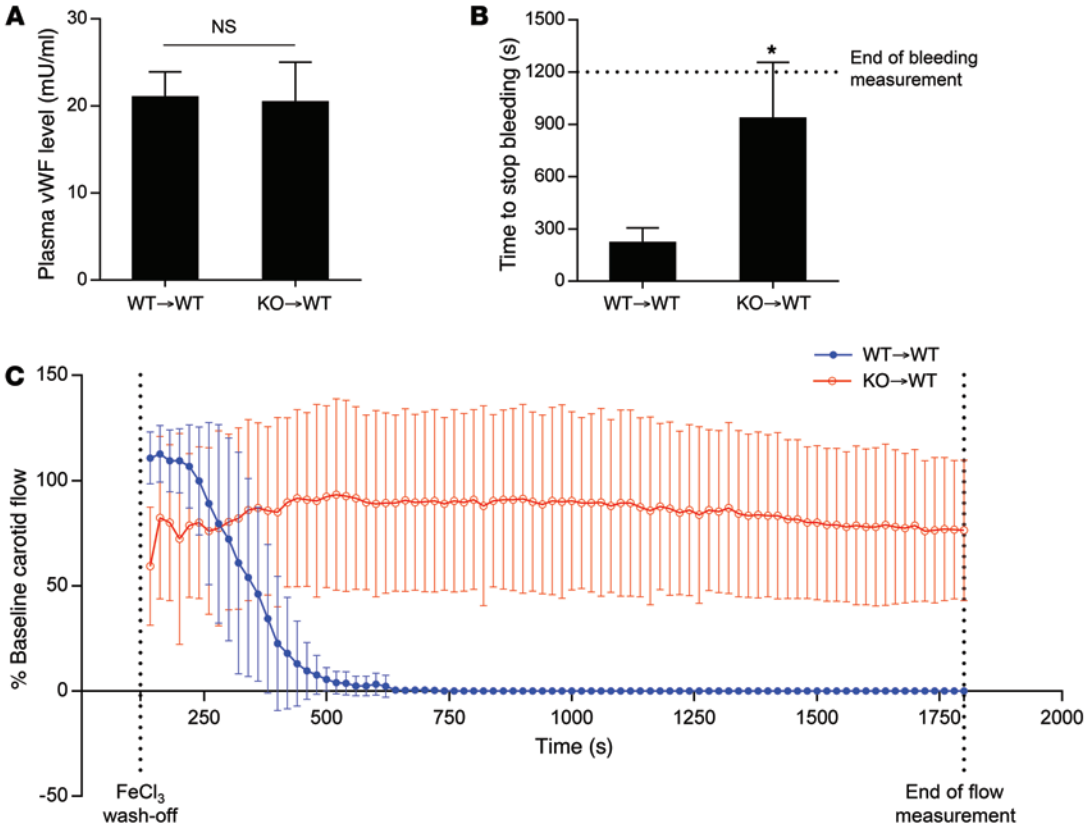

Figure 8. STXBP5 in platelets increases thrombosis in mice. BM from WT or *Stxbp5* KO mice was transplanted into lethally irradiated WT recipients (WT→WT and KO→WT, respectively), and experiments were performed 6 weeks after transplantation. Transplantation of *Stxbp5* KO BM did not affect plasma vWF levels (n = 7–9; **A**), increased tail bleeding time (n = 7–9; **B**), and decreased carotid arterial thrombosis (n = 6–7; **C**; $FeCl_3$ injury as in Figure 6C). All data are mean ± SD. *$P < 0.05$.

basal release, and unstimulated constitutive release (79). However, the proteins that mediate unstimulated release have not been defined, and it is unknown which proteins regulate both the unstimulated release pathway and the stimulated pathway. Our data suggest that STXBP5 acts upon 1 or more proteins in the stimulated secretory pathway. For example, we found STXBP5 to interact with STX4. Furthermore, others have shown that in neurons, STXBP5 interacts with SYT1, whose regulatory role in exocytosis depends on calcium (68).

One striking finding of our study was that STXBP5 had opposing effects on exocytosis from ECs and platelets, inhibiting the former while activating the latter. Platelets from *Stxbp5* KO mice had impaired secretion of α granules (as measured by P-selectin externalization), defective exocytosis of dense granules (as measured by ATP release), and blunted activation (as measured by GPIIbIIIα conformational changes) (Figure 7B). Furthermore, mice lacking *Stxbp5* displayed severe defects in bleeding time, mesenteric arteriole thrombosis, and carotid artery thrombosis. BM transplant experiments suggested that this hemostasis defect is caused by BM-derived cells (presumably platelets, not ECs) lacking STXBP5 (Figure 8).

Why did STXBP5 promote platelet exocytosis, but suppress endothelial exocytosis? We considered the idea that platelets and ECs express different isoforms of STXBP5, but our PCR findings showed that both cell types expressed predicted *STXBP5* transcript variants with similar relative abundance (Figure 1D). Another possibility is that STXBP5 interacts with different SNARE members in different cell types. Although STXBP5 interacted with STX4 and SYT1 in ECs (Figure 4), it did not significantly interact with STX4 or SYT1 in human platelets (data not shown) or with STX4 in rat brain (49, 50). Others have reported divergent effects of STXBP5 in differing cell systems. For example, STXBP5 inhibits neurotransmitter release from neurons (55–61), but actually increases the readily releasable pool of vesicles in PC12 cells and in rat β cell line INS-1E; this stimulation of exocytosis depends in part on STXBP5 phosphorylation (60, 80). Detailed studies of molecular mechanisms are needed to reconcile the paradoxically stimulatory and inhibitory dual roles of STXBP5.

Mice lacking *Stxbp5* had increased plasma levels of vWF, but decreased thrombosis. Why? Our data suggest that STXBP5 has opposing effects on endothelial and platelet exocytosis. In *Stxbp5* KO mice, the increased plasma vWF was caused by the absence of endothelial STXBP5 that normally limits endothelial release of vWF. Since the major source of vWF in mouse plasma is ECs, not platelets (81), mice lacking *Stxbp5* in both ECs and platelets demonstrated increased plasma vWF. Our data using BM transplanted mice supported this conclusion, since plasma vWF levels were unchanged by BM from *Stxbp5* KO donors (Figure 8). In *Stxbp5* KO mice, the decreased thrombosis was caused by the absence of platelet STXBP5, which normally boosts platelet activation. The

enhanced plasma vWF was not sufficient to overcome the diminished platelet activation, and the net result of STXBP5 absence from both ECs and platelets was defective thrombosis. Thus, STXBP5 has a previously unrecognized effect on platelet activation, and this effect on platelets appears to be dominant over the effect on ECs for thrombosis.

Human GWAS show that multiple genetic variants associated with altered vWF levels lie within the *STXBP5* allele (45–47). One SNP highly correlated with altered vWF levels in humans, rs1039084, is located in exon 13 of *STXBP5* (47). This nonsynonymous SNP changes 1,307 A to G in *STXBP5*, changing codon 436 from Asn to Ser (N436S). Human studies have found that the N436S STXBP5 mutation is associated with lower levels of vWF in the plasma (47).

Our present studies matched the GWAS findings: N436S STXBP5 decreased endothelial exocytosis more than WT STXBP5 (Supplemental Figure 4). Residue N436 lies within the N-terminal WD40 repeat domain of STXBP5. WD40 repeats can form scaffolds that assemble protein complexes, and we have previously shown that the STXBP5 WD40 repeat domain interacts with the SNAREs STX1 and SNAP25 in neurons (56). How might the N436S STXBP5 mutation enhance inhibition of exocytosis? It is possible that N436S STXBP5 enhances the affinity of STXBP5 for STX4 in ECs, blocking the formation of a ternary SNARE complex. Another possibility is that the mutation decreases the conformational changes that might permit STXBP5 to release SNAREs to form the ternary SNARE complex. Or perhaps the N436S STXBP5 mutation serves as a gain-of-function mutation that mediates the interaction of STXBP5 with additional partners.

Genetic variation within *STXBP5* is linked to the risk of venous thromboembolic events in human subjects (48). The effect of the mutation N436S STXBP5 upon platelet activation is unknown. We found that N436S STXBP5 enhanced the function of STXBP5 in ECs, with enhanced suppression of exocytosis (Supplemental Figure 4). We would expect that the mutation would also enhance the function of STXBP5 in platelets, with further promotion of platelet activation. However, in human studies, the SNP rs1039084 for N436S STXBP5 is associated with decreased incidence of venous thromboembolic disease (48). It is possible that different partners interacting with STXBP5 in platelets and ECs determines the effect of the N436S STXBP5 mutation. Further studies are needed to determine the effect of mutations on STXBP5 function in platelets.

In conclusion, our present data identified a key role for STXBP5 as a novel regulator in endothelial exocytosis and thrombosis. STXBP5 inhibited stimulated endothelial release of vWF and translocation of P-selectin in vitro. It colocalized with endothelial vesicles and formed complexes with the endothelial SNAREs STX4 and SYT1. Moreover, *Stxbp5* deficiency in mice significantly increased plasma vWF levels and P-selectin translocation. However, STXBP5 also promoted platelet secretion, and mice lacking *Stxbp5* had increased bleeding. The effect of STXBP5 on platelets was dominant to its effect on ECs for thrombosis. Our studies are relevant to humans, since human GWAS data associates *STXBP5* genetic variants with plasma vWF levels and thrombosis. Further characterization of the regulatory functions of STXBP5 in exocytosis may lead to novel insights into vascular diseases such as venous thromboembolism and von Willebrand disease.

Methods

Antibodies and reagents. Primary and secondary antibodies used for this study are listed in Supplemental Table 1. Lipofectin reagent and Opti-MEM I media were purchased from Invitrogen. Protease Inhibitor Cocktail (Complete Mini EDTA-free) was purchased from Roche. The Ca^{2+} ionophore A23187, $FeCl_3$, histamine, thrombin, and ATP were purchased from Sigma-Aldrich.

Cell culture and transfection. HUVECs, HAECs, HDMVECs, and EC culture medium containing EC growth supplement (VascuLife EnGS) were obtained from Lifeline Cell Technology. ECs were maintained in collagen I–coated plates, and passages 3–6 were used for all in vitro studies. The HL-60 promyelocytic cell line was purchased from American Type Culture Collection. Human platelets were isolated from whole blood of healthy donors free of nonsteroidal antiinflammatory drugs for at least 10 days, as previously described (82). Transfection was performed at 80%–90% confluence using Lipofectin reagent following the manufacturer's protocol (Invitrogen), with either 0.5 μg/ml plasmid DNA or 20 nM siRNA oligonucleotides (Applied Biosystems). Cells were stimulated or imaged at least 72 hours after transfection.

vWF release assay. Confluent HUVECs, HAECs, and HDMVECs were stimulated with 10 μM histamine, 10 μM A23187, 10 μM ATP, or sham treatment (PBS) for 30 minutes at 37°C to stimulate vWF release. After stimulation of the cells, vWF concentration in the cell media was quantified by a vWF ELISA kit (American Diagnostica Inc. and Sekisui Diagnostics LLC). In separate experiments, HUVECs transfected with control or STXBP5 siRNA were lysed without stimulation, and intracellular vWF contents were measured in an equal amount of protein lysate. We found the antibody against vWF in this ELISA cross-reacted with mouse vWF antigen. Separate measurements were performed in diluted mouse plasma collected by retroorbital bleeding from littermate WT and *Stxbp5* KO mice.

EC-leukocyte interaction. Adhesion of neutrophils to HUVECs was performed as described previously (36, 43, 44). HUVECs were transfected with control siRNA or siRNA against STXBP5 in a 12-well plate, then cultured until 100% confluent. Prior to the adhesion assay, HL-60 cells were labeled with 2 μM Calcein AM (Molecular Probes) for 30 minutes at 37°C, washed, and suspended in serum-free media. Then 1×10^5 HL-60 cells in 500 μl serum-free media were added to each well in the presence or absence of 10 μM histamine. The plate was kept at 4°C for 15 minutes, washed twice with HBSS, refilled with media, and immediately imaged with an Olympus BX51 upright microscope with a ×10 water immersion objective. Cells preincubated with an azide-free antibody raised against full-length P-selectin (AK4) was used as negative control.

ADAMTS13 assay. We used an assay to measure ADAMTS13 in murine plasma (83). S. Neelamegham (State University of New York at Buffalo, Buffalo, New York, USA) provided a recombinant polypeptide, XS-vWF, which contains a truncated fragment of the vWF-A2 domain cleavable by ADAMTS13. This polypeptide is flanked by a CFP variant Cerulean and an YFP variant Venus that exhibit fluorescence/Förster resonance energy transfer (FRET) properties. ADAMTS13 cleavage of XS-vWF keeps the fluophores apart, increasing Cerulean emission and decreasing FRET efficiency. ADAMTS13 activity was quantified by the FRET ratio, defined as the ratio of Cerulean/Venus emission at 420 nm. We found that mouse plasma efficiently cleaved XS-vWF. In this assay, 15 μl WT or *Stxbp5* KO mouse plasma were incubated with 10 μl XS-vWF substrate in 100 μl cleavage buffer (50 mM Tris, pH 8.0, and 12.5 mM $CaCl_2$) in a 96-well plate for 1 hour at 37°C. The FRET

ratio was measured on a plate reader, and ADAMTS13 activity was calculated as the percentage of pooled WT mouse plasma.

Western blotting. Western blotting was performed as described previously (35). In brief, ECs or platelets were lysed with Laemmli sample buffer (Bio-Rad), boiled for 5 minutes at 95°C, resolved on 4% to 20% Mini-PROTEAN TGX Precast gels (Bio-Rad), and transferred using a Trans-Blot SD semidry electrophoretic transfer unit (Bio-Rad) onto nitrocellulose membranes. After 1 hour of blocking with 5% nonfat milk in PBS containing 0.05% Tween 20 at room temperature, the membranes were hybridized with primary antibodies, followed by HRP-conjugated secondary antibodies and enhanced chemiluminescence detection using X-ray films.

qPCR. Murine tissue was harvested immediately after transcardial perfusion with diethylpyrocarbonate-treated PBS. Total RNA was isolated with TRIzol following the manufacture's protocol (Invitrogen) and purified with lithium chloride (Sigma-Aldrich). The A260/A280 ratio of all samples was 1.9–2.1, as measured by spectrophotometry (NanoDrop; Thermo Scientific). cDNA was synthesized using an iScript cDNA Synthesis kit (Bio-Rad). qPCR was performed by Taqman gene expression assay (Applied Biosystems) for 40 cycles on an iCycler thermal cycler equipped with MyiQ PCR detection system (Bio-Rad). For each organ, 3 independent experiments were performed, and in each experiment TaqMan quantification was repeated in triplicate for each sample. Taqman probes were purchased from Applied Biosystems. For each probe set, calibration curves were generated by 10-fold serial dilutions of cDNA to ensure comparable PCR efficiency. Expression results were calculated by ΔΔCt and normalized to the reference genes *GAPDH* or *Gapdh*.

Identification of STXBP5 mRNA splice variants. Primers flanking the splice region of human *STXBP5* mRNAs were designed (5′-TCGCTGCAAATCTCCAACCT-3′ and 5′-GGACGAGTCCGTCTTTCGAG-3′). HUVECs, human platelets, and HEK293 cDNA were synthesized as described above. Human adult brain cDNA was purchased from Biochain. PCR was performed using 0.25 μg cDNA per reaction with the above primers. The products were separated by agarose gel, sequenced, and compared with validated and predicted NCBI reference sequences. 5 NCBI sequences were found to match the sequencing results: NM_001127715.2, NM_139244.4, XR_245502.1, XR_245503.1, and XR_245504.1. Quantification of each splice variant was performed using custom Taqman probes, each spanning exon boundaries specific for 1 splice variant (NM_001127715.2, exons 21–23; NM_139244.4, exons 19–23; XR_245502.1, exons 21–22; XR_245503.1, exons 20–22; XR_245504.1, exons 19–22).

Site-directed mutagenesis. Mouse pMEX neo-3×FLAG-tomosyn (8)-ATG expression plasmid was provided by D.E. James (Garvan Institute of Medical Research, Darlinghurst, New South Wales, Australia) (84). A point mutation corresponding to human SNP rs1039084 (A→G) was introduced by site-directed mutagenesis with a QuikChange Mutagenesis Kit (Agilent Technologies). Using the plasmid as template, PCR was performed with the following primers for mutagenesis: 5′-AAAGGAATGGCCCATCAGCGGAGGTAATTGGGGCTT-3′ and 5′-AAGCCCCAATTACCTCCGCTGATGGGCCATTCCTTT-3′. PCR products were treated by DpnI to digest template plasmid, then transformed into competent cells. The mutated plasmid was extracted using EndoFree Plasmid Maxi Kit (Qiagen), and mutation was confirmed by DNA sequencing.

Coimmunoprecipitation of STXBP5 and its interacting proteins. HUVECs were lysed with coimmunoprecipitation buffer containing 10 mM HEPES/NaOH (pH 7.4), 140 mM NaCl, 5 mM $NaHCO_3$, 1.2 mM NaH_2PO_4, 1 mM $MgCl_2$, 10 mM glucose, 5 mM KCl, 1 mM EGTA, 1.3 mM $CaCl_2$, and 1% (w/v) Triton X-100 supplemented with protease inhibitor cocktails on ice and incubated for 60 minutes, followed by centrifugation at 161,000 *g* at 4°C for 20 minutes. 25 μl Protein A/G PLUS-Agarose was incubated with 2 μg mouse anti-STXBP5 antibody or mouse IgG_1 at 4°C overnight, washed, and then mixed with the precleared cell lysate at 4°C overnight. The precipitants were washed with cold coimmunoprecipitation buffer 6 times, and the bound proteins were then solubilized in reducing Laemmli sample buffer at 95°C. The elute was resolved by SDS-PAGE followed by IB.

Confocal microscopy. HUVECs were cultured on collagen-coated 35-mm glass dishes (MatTek). After removal of media, cells were rinsed twice with PBS and fixed immediately with 4% PFA for 20 minutes. After permeabilization with 0.15% Triton X-100 for 10 minutes and blocking with 5% donkey serum for 1 hour at room temperature, cells were incubated with primary antibodies (1:100–1:330 dilution) overnight at 4°C followed by 1 hour of incubation at room temperature with fluorescent secondary antibodies (1:2,000 dilution) and DAPI. Fluorescence microscopy was performed using an IX81 inverted confocal microscope equipped with a high-sensitivity digital camera (FV1000; Olympus). All fluorescent images were generated using sequential line scanning with identical settings in each experiment at maximum *z* resolution (0.40 μm for ×40 objective, 0.32 μm for ×60 objective). Image analysis was carried out using FV10-ASW 3.0 (Olympus) and Image-Pro Plus (Media Cybernetics).

Sucrose density gradient ultracentrifugation. HUVECs were lysed on ice with 2 ml coimmunoprecipitation buffer supplemented with protease inhibitor cocktails and incubated for 1 hour at 4°C followed by centrifugation at 161,000 *g* for 20 minutes. The supernatant was carefully loaded on top of a discontinuous sucrose density gradient of 1 ml 5% sucrose, 6 ml 30% sucrose, and 3 ml 40% sucrose in coimmunoprecipitation buffer (from top to bottom) in a 14 ml PET thin-walled tube (Thermo Scientific). The sucrose density gradient was then ultracentrifuged at 166,880 *g* for 20 hours at 4°C on a Discovery 100s ultracentrifugation equipped with a SureSpin 630/17 swinging-bucket rotor (Sorvall). After ultracentrifugation, 18 equal-volume aliquots were carefully aspirated from top to bottom, boiled in equal-volume 2× sample loading buffer, and analyzed by 7.5% SDS-PAGE.

Animal models. *Stxbp5* KO mice (provided by J. Miyoshi, Osaka University, Osaka, Japan) on a 50% 129Sv, 25% C57BL/6, and 25% DBA/2 background were generated as previously described (56). PCR was used for genotyping with primers specific for a WT allele (5′-TTCTGCTCCCCGCTGCTCCTT-3′ and 5′-TCCCCGCTCCCTTCACCTTGC-3′) and a mutant allele (5′-GGGCGCCCGGTTCTTTTTGTC-3′ and 5′-GCCATGATGGATACTTTCTCG-3′). The PCR products for the WT and mutant alleles were 300 and 224 bp, respectively. We used 4- to 8-week-old male *Stxbp5* KO mice and WT littermates for all in vivo experiments, unless otherwise specified.

Platelet isolation and activation. Murine blood was obtained by retroorbital bleeding of anesthetized animal into heparinized murine Tyrode's buffer (134 mM NaCl; 2.9 mM KCl; 12 mM $NaHCO_3$; 0.34 mM Na_2HPO_4; 20 mM HEPES, pH 7.0; 5 mM glucose; and 0.35% bovine serum albumin) in Eppendorf tubes. The blood was centrifuged to yield platelet-rich plasma, which was then washed in new tubes containing Tyrode's buffer with 1% PGE_2 to prevent platelet activation. Platelets were then pelleted by centrifugation for 5 minutes at 600 *g* at room tem-

perature, and the supernatant was discarded. The pelleted platelets were gently resuspended in Tyrode's buffer and kept at room temperature for further experiments within 2 hours. For platelet activation, diluted platelet suspension was divided into 100-μl aliquots (3 per agonist per mouse), stimulated with 10 μl PBS or thrombin for 10 minutes, stained with 2 μl FITC-conjugated CD62 antibody and 4 μl PE-conjugated JonA antibody for 15 minutes, and immediately fixed with 100 μl 2% formalin. Fluorescence intensity was measured on an Accuri C6 Flow Cytometer (BD Biosciences). Data were analyzed with FlowJo software (Tree Star Inc.) using single-stained nonactivated WT platelets for fluorescence compensation. ATP release was measured in poststimulation supernatant using an ATP Bioluminescent Assay Kit (Sigma-Aldrich).

Platelet adherence assay. Mice were anesthetized with a cocktail of ketamine/xylazine (80:12 mg/kg) and saline (10 ml/kg) via i.m. injection. Anesthetized mice were injected with a DyLight488 antibody against GPIbβ to label platelets. For platelet adherence assay, the mesentery was exteriorized on a petri dish and then placed on an inverted fluorescent intravital microscope (ECLIPSE Ti; Nikon) with a 37°C stage warmer. An area containing target venules (120–150 μm in diameter) was selected. After 120-second baseline recording, the mesenteric venules were superfused with 10 μM A23187 to activate ECs and to induce platelet rolling. Images of platelets rolling in the mesenteric venules were continuously recorded for a total of 10 minutes starting at the baseline with an electron-multiplying CCD video camera (512SC; QUANTEM). Using Image-Pro Plus software, platelet rolling was determined by counting the number of platelets that remained static for at least 2 consecutive images. For each mouse, we quantified platelet rolling in 5 equally distributed video segments (1 during baseline and 4 during stimulation), each 500 frames in length, and used the average number of rolling platelets per unit time per unit area (512 pixels × 100 pixels) for quantification.

In vivo P-selectin exocytosis assay. Yellow-green fluorescent 1-μm microspheres (Invitrogen) were coupled to anti-mouse CD62P antibody. Anesthetized mice were infused with 10^8 microspheres i.v., and the mesentery was externalized as described above. Intravital microscopy was used to visualize fluorescent microspheres binding to unstimulated venules for 2 minutes, followed by 8 minutes of stimulation by A23187. For each mouse, P-selectin exocytosis was determined by counting the number of adherent microspheres on each frame of a 100-frame cropped video and averaged over the resting and stimulation conditions. The adherent number of microspheres per unit area (512 pixel × 100 pixel) was used for quantification.

Mouse tail bleeding assay. Mouse tail bleeding time was measured as described previously (85). After i.p. anesthetization with ketamine/xylazine (80:12 mg/kg), the distal 5 mm of the mouse tail was amputated and immersed immediately in 37°C saline, and the time to visual cessation of bleeding (30 seconds duration) or continuous bleeding (20 minutes maximal duration), whichever occurred first, was recorded.

Mouse mesenteric and carotid thrombosis model. These models were as described previously (86, 87). For the mesenteric thrombosis model, mice were anesthetized and platelets labeled with DyLight488-antibody against GPIbβ. A target area containing mesenteric arterioles (120–150 μm in diameter) was externalized for imaging. The arteriole flow was recorded for 3 minutes at resting condition. Then 1 mm^2 of Whatman paper saturated with 7.5% $FeCl_3$ solution was applied to the arteriole for 3 minutes, and the arteriole flow was continuously recorded for a total of 30 minutes. The time to form a small thrombus (50-pixel diameter) and to full vessel occlusion were recorded. Recording was terminated at the end of 30 minutes if no occlusion was observed. For the carotid thrombosis model, mice were sedated with 2.5% isoflurane and kept anesthetized with 2% isoflurane. The common carotid arteries were exposed for a baseline flow recording using an MA1PRB Perivascular Flowprobe and a TS420 Flowmeter (Transonic Systems). Next, 1 mm × 2 mm Whatman paper soaked with 1.5 μl 7.5% $FeCl_3$ solution was applied to the ventral surface of the carotid upstream of the flowprobe for 3 minutes. Flow measurement was resumed for a total of 30 minutes after $FeCl_3$ wash-off. We defined occlusion as the absence of blood flow (0 ml/min) for 3 minutes.

BM transplantation. WT and *Stxbp5* KO BM donor mice were euthanized, and femurs were isolated under sterile conditions. BM was harvested and then aspirated repeatedly to create single-cell suspensions. Cell counts were manually performed, and 10^7 cells were injected into each recipient mouse i.v. via the retroorbital plexus on the same day as lethal irradiation of recipients. WT 8-week-old mice were used as recipients and were lethally irradiated with an X-ray RS 2000 (Rad-sources) irradiator delivering a single dose of 11 Gy. After BM transplantation, mice were provided with water supplemented with sulfatrim for 2 weeks and allowed to reconstitute for 6 weeks prior to tail bleeding assay, blood collection, and carotid injury.

Statistics. Data were analyzed by 2-tailed Student's *t* test for comparison of 2 groups and by 1-way ANOVA to compare means of 3 or more groups. A *P* value less than 0.05 was considered significant.

Study approval. All in vivo procedures and usage of mice were approved by the Division of Laboratory Animal Medicine at the University of Rochester Medical Center.

Acknowledgments

We thank Jun Miyoshi for *Stxbp5* KO mice, Sriram Neelamegham for XS-vWF protein, and David James for pMEX neo-3×FLAG-tomosyn (8)-ATG expression plasmid. This work was supported by NIH/NHLBI grant R21 HL108372 (to C.J. Lowenstein); by the HHMI "Med-into-Grad" Fellowship in Cardiovascular Sciences at the Aab Cardiovascular Research Institute, University of Rochester (to C.J. Lowenstein and Q. Zhu); and by American Heart Association grants 14GRNT19020033 (to C.J. Lowenstein), 0835446N (to M. Yamakuchi), and 13PRE17050105 (to Q. Zhu).

Address correspondence to: Charles J. Lowenstein, Box CVRI, 601 Elmwood Avenue, Rochester, New York 14642, USA. Phone: 585.276.5077; E-mail: charles_lowenstein@urmc.rochester.edu.

1. Furie B, Furie BC. Mechanisms of thrombus formation. *N Engl J Med*. 2008;359(9):938–949.
2. Wells PS, Forgie MA, Rodger MA. Treatment of venous thromboembolism. *JAMA*. 2014;311(7):717–728.
3. Farge D, et al. International clinical practice guidelines for the treatment and prophylaxis of venous thromboembolism in patients with cancer. *J Thromb Haemost*. 2013;11(1):56–70.
4. Wagner DD, Frenette PS. The vessel wall and its interactions. *Blood*. 2008;111(11):5271–5281.
5. Mackman N. Triggers, targets and treatments for thrombosis. *Nature*. 2008;451(7181):914–918.
6. Ignarro LJ, Buga GM, Wood KS, Byrns RE, Chaudhuri G. Endothelium-derived relaxing factor produced and released from artery and vein is nitric oxide. *Proc Natl Acad Sci U S A*. 1987;84(24):9265–9269.

7. Palmer RM, Ferrige AG, Moncada S. Nitric oxide release accounts for the biological activity of endothelium-derived relaxing factor. *Nature*. 1987;327(6122):524–526.
8. Marcus AJ, Broekman MJ, Pinsky DJ. COX inhibitors and thromboregulation. *N Engl J Med*. 2002;347(13):1025–1026.
9. Marcus AJ, et al. Role of CD39 (NTPDase-1) in thromboregulation, cerebroprotection, and cardioprotection. *Semin Thromb Hemost*. 2005;31(2):234–246.
10. Lowenstein CJ, Morrell CN, Yamakuchi M. Regulation of Weibel-Palade body exocytosis. *Trends Cardiovasc Med*. 2005;15(8):302–308.
11. Weibel ER, Palade GE. New cytoplasmic components in arterial endothelia. *J Cell Biol*. 1964;23:101–112.
12. Bergmeier W, Chauhan AK, Wagner DD. Glycoprotein Ibalpha and von Willebrand factor in primary platelet adhesion and thrombus formation: lessons from mutant mice. *Thromb Haemost*. 2008;99(2):264–270.
13. Wagner DD. The Weibel-Palade body: the storage granule for von Willebrand factor and P-selectin. *Thromb Haemost*. 1993;70(1):105–110.
14. Calvert JW, et al. Inhibition of N-ethylmaleimide-sensitive factor protects against myocardial ischemia/reperfusion injury. *Circ Res*. 2007;101(12):1247–1254.
15. Yamakuchi M, et al. HMG-CoA reductase inhibitors inhibit endothelial exocytosis and decrease myocardial infarct size. *Circ Res*. 2005;96(11):1185–1192.
16. Goodman DM, Burke AE, Livingston EH. JAMA patient page. Bleeding disorders. *JAMA*. 2012;308(14):1492.
17. Thompson SG, Kienast J, Pyke SD, Haverkate F, van de Loo JC. Hemostatic factors and the risk of myocardial infarction or sudden death in patients with angina pectoris. European Concerted Action on Thrombosis and Disabilities Angina Pectoris Study Group. *N Engl J Med*. 1995;332(10):635–641.
18. Spiel AO, Gilbert JC, Jilma B. von Willebrand factor in cardiovascular disease: focus on acute coronary syndromes. *Circulation*. 2008;117(11):1449–1459.
19. Vischer UM. von Willebrand factor, endothelial dysfunction, and cardiovascular disease. *J Thromb Haemost*. 2006;4(6):1186–1193.
20. Jahn R, Sudhof TC. Membrane fusion and exocytosis. *Annu Rev Biochem*. 1999;68:863–911.
21. Rothman JE. Mechanisms of intracellular protein transport. *Nature*. 1994;372(6501):55–63.
22. Bajjalieh SM, Scheller RH. Synaptic vesicle proteins and exocytosis. *Adv Second Messenger Phosphoprotein Res*. 1994;29:59–79.
23. Sudhof TC. The synaptic vesicle cycle: a cascade of protein-protein interactions. *Nature*. 1995;375(6533):645–653.
24. Jahn R, Scheller RH. SNAREs — engines for membrane fusion. *Nat Rev Mol Cell Biol*. 2006;7(9):631–643.
25. Sudhof TC. The synaptic vesicle cycle revisited. *Neuron*. 2000;28(2):317–320.
26. Martens S, McMahon HT. Mechanisms of membrane fusion: disparate players and common principles. *Nat Rev Mol Cell Biol*. 2008;9(7):543–556.
27. Pulido IR, Jahn R, Gerke V. VAMP3 is associated with endothelial Weibel-Palade bodies and participates in their Ca^{2+}-dependent exocytosis. *Biochim Biophys Acta*. 2011;1813(5):1038–1044.
28. Jung JJ, Tiwari A, Inamdar SM, Thomas CP, Goel A, Choudhury A. Secretion of soluble vascular endothelial growth factor receptor 1 (sVEGFR1/sFlt1) requires Arf1, Arf6, and Rab11 GTPases. *PLoS One*. 2012;7(9):e44572.
29. van Hooren KW, van Agtmaal EL, Fernandez-Borja M, van Mourik JA, Voorberg J, Bierings R. The Epac-Rap1 signaling pathway controls cAMP-mediated exocytosis of Weibel-Palade bodies in endothelial cells. *J Biol Chem*. 2012;287(29):24713–24720.
30. Yamakuchi M, et al. Exocytosis of endothelial cells is regulated by N-ethylmaleimide-sensitive factor. *Methods Mol Biol*. 2008;440:203–215.
31. Bierings R, et al. The interplay between the Rab27A effectors Slp4-a and MyRIP controls hormone-evoked Weibel-Palade body exocytosis. *Blood*. 2012;120(13):2757–2767.
32. Pulido IR, Nightingale TD, Darchen F, Seabra MC, Cutler DF, Gerke V. Myosin Va acts in concert with Rab27a and MyRIP to regulate acute von-Willebrand factor release from endothelial cells. *Traffic*. 2011;12(10):1371–1382.
33. Nightingale TD, Pattni K, Hume AN, Seabra MC, Cutler DF. Rab27a and MyRIP regulate the amount and multimeric state of VWF released from endothelial cells. *Blood*. 2009;113(20):5010–5018.
34. Kim KS, Park JY, Jou I, Park SM. Regulation of Weibel-Palade body exocytosis by alpha-synuclein in endothelial cells. *J Biol Chem*. 2010;285(28):21416–21425.
35. Matsushita K, et al. Nitric oxide regulates exocytosis by S-nitrosylation of N-ethylmaleimide-sensitive factor. *Cell*. 2003;115(2):139–150.
36. Ito T, Yamakuchi M, Lowenstein CJ. Thioredoxin increases exocytosis by denitrosylating N-ethylmaleimide-sensitive factor. *J Biol Chem*. 2011;286(13):11179–11184.
37. Huang J, Motto DG, Bundle DR, Sadler JE. Shiga toxin B subunits induce VWF secretion by human endothelial cells and thrombotic microangiopathy in ADAMTS13-deficient mice. *Blood*. 2010;116(18):3653–3659.
38. Liu F, Huang J, Sadler JE. Shiga toxin (Stx)1B and Stx2B induce von Willebrand factor secretion from human umbilical vein endothelial cells through different signaling pathways. *Blood*. 2011;118(12):3392–3398.
39. Knipe L, et al. A revised model for the secretion of tPA and cytokines from cultured endothelial cells. *Blood*. 2010;116(12):2183–2191.
40. Into T, et al. Pathogen recognition by Toll-like receptor 2 activates Weibel-Palade body exocytosis in human aortic endothelial cells. *J Biol Chem*. 2007;282(11):8134–8141.
41. Bhatia R, Matsushita K, Yamakuchi M, Morrell CN, Cao W, Lowenstein CJ. Ceramide triggers Weibel-Palade body exocytosis. *Circ Res*. 2004;95(3):319–324.
42. Matsushita K, Morrell CN, Lowenstein CJ. Sphingosine 1-phosphate activates Weibel-Palade body exocytosis. *Proc Natl Acad Sci U S A*. 2004;101(31):11483–11487.
43. Jeong Y, et al. Aldosterone activates endothelial exocytosis. *Proc Natl Acad Sci U S A*. 2009;106(10):3782–3787.
44. Yamakuchi M, et al. Antibody to human leukocyte antigen triggers endothelial exocytosis. *Proc Natl Acad Sci U S A*. 2007;104(4):1301–1306.
45. Smith NL, et al. Novel associations of multiple genetic loci with plasma levels of factor VII, factor VIII, and von Willebrand factor: The CHARGE (Cohorts for Heart and Aging Research in Genome Epidemiology) Consortium. *Circulation*. 2010;121(12):1382–1392.
46. Antoni G, et al. Combined analysis of three genome-wide association studies on vWF and FVIII plasma levels. *BMC Med Genet*. 2011;12:102.
47. van Loon JE, et al. Effect of genetic variations in syntaxin-binding protein-5 and syntaxin-2 on von Willebrand factor concentration and cardiovascular risk. *Circ Cardiovasc Genet*. 2010;3(6):507–512.
48. Smith NL, et al. Genetic variation associated with plasma von Willebrand factor levels and the risk of incident venous thrombosis. *Blood*. 2011;117(22):6007–6011.
49. Fujita Y, et al. Tomosyn: a syntaxin-1-binding protein that forms a novel complex in the neurotransmitter release process. *Neuron*. 1998;20(5):905–915.
50. Yokoyama S, Shirataki H, Sakisaka T, Takai Y. Three splicing variants of tomosyn and identification of their syntaxin-binding region. *Biochem Biophys Res Commun*. 1999;256(1):218–222.
51. Groffen AJ, Jacobsen L, Schut D, Verhage M. Two distinct genes drive expression of seven tomosyn isoforms in the mammalian brain, sharing a conserved structure with a unique variable domain. *J Neurochem*. 2005;92(3):554–568.
52. Pobbati AV, Razeto A, Boddener M, Becker S, Fasshauer D. Structural basis for the inhibitory role of tomosyn in exocytosis. *J Biol Chem*. 2004;279(45):47192–47200.
53. Hatsuzawa K, Lang T, Fasshauer D, Bruns D, Jahn R. The R-SNARE motif of tomosyn forms SNARE core complexes with syntaxin 1 and SNAP-25 and down-regulates exocytosis. *J Biol Chem*. 2003;278(33):31159–31166.
54. Masuda ES, Huang BC, Fisher JM, Luo Y, Scheller RH. Tomosyn binds t-SNARE proteins via a VAMP-like coiled coil. *Neuron*. 1998;21(3):479–480.
55. Yizhar O, et al. Multiple functional domains are involved in tomosyn regulation of exocytosis. *J Neurochem*. 2007;103(2):604–616.
56. Sakisaka T, et al. Dual inhibition of SNARE complex formation by tomosyn ensures controlled neurotransmitter release. *J Cell Biol*. 2008;183(2):323–337.
57. Yizhar O, et al. Tomosyn inhibits priming of large dense-core vesicles in a calcium-dependent manner. *Proc Natl Acad Sci U S A*. 2004;101(8):2578–2583.
58. Yamamoto Y, et al. The tail domain of tomosyn controls membrane fusion through tomosyn displacement by VAMP2. *Biochem Biophys Res Commun*. 2010;399(1):24–30.
59. Williams AL, et al. Structural and functional analysis of tomosyn identifies domains important in exocytotic regulation. *J Biol Chem*. 2011;286(16):14542–14553.
60. Baba T, Sakisaka T, Mochida S, Takai Y. PKA-catalyzed phosphorylation of tomosyn and its

implication in Ca^{2+}-dependent exocytosis of neurotransmitter. *J Cell Biol.* 2005;170(7):1113–1125.
61. Gladycheva SE, et al. Receptor-mediated regulation of tomosyn-syntaxin 1A interactions in bovine adrenal chromaffin cells. *J Biol Chem.* 2007;282(31):22887–22899.
62. Mcever RP, Beckstead JH, Moore KL, Marshallcarlson L, Bainton DF. GMP-140, a platelet α-granule membrane protein, is also synthesized by vascular endothelial cells and is localized in Weibel-Palade bodies. *J Clin Invest.* 1989;84(1):92–99.
63. Hagedorn I, Vogtle T, Nieswandt B. Arterial thrombus formation. Novel mechanisms and targets. *Hamostaseologie*. 2010;30(3):127–135.
64. Stoll G, Kleinschnitz C, Nieswandt B. Molecular mechanisms of thrombus formation in ischemic stroke: novel insights and targets for treatment. *Blood*. 2008;112(9):3555–3562.
65. Falanga A, Marchetti M, Vignoli A, Balducci D. Clotting mechanisms and cancer: implications in thrombus formation and tumor progression. *Clin Adv Hematol Oncol*. 2003;1(11):673–678.
66. Fu J, Naren AP, Gao X, Ahmmed GU, Malik AB. Protease-activated receptor-1 activation of endothelial cells induces protein kinase Cα-dependent phosphorylation of syntaxin 4 and Munc18c: role in signaling p-selectin expression. *J Biol Chem*. 2005;280(5):3178–3184.
67. Valentijn KM, Sadler JE, Valentijn JA, Voorberg J, Eikenboom J. Functional architecture of Weibel-Palade bodies. *Blood*. 2011;117(19):5033–5043.
68. Yamamoto Y, et al. Tomosyn inhibits synaptotagmin-1-mediated step of Ca^{2+}-dependent neurotransmitter release through its N-terminal WD40 repeats. *J Biol Chem.* 2010;285(52):40943–40955.
69. Savage B, Ginsberg MH, Ruggeri ZM. Influence of fibrillar collagen structure on the mechanisms of platelet thrombus formation under flow. *Blood*. 1999;94(8):2704–2715.
70. van Loon JE, Sanders YV, de Wee EM, Kruip MJ, de Maat MP, Leebeek FW. Effect of genetic variation in STXBP5 and STX2 on von Willebrand factor and bleeding phenotype in type 1 von Willebrand disease patients. *PLoS One.* 2012;7(7):e40624.
71. McEwen JM, Madison JM, Dybbs M, Kaplan JM. Antagonistic regulation of synaptic vesicle priming by Tomosyn and UNC-13. *Neuron*. 2006;51(3):303–315.
72. Grosshans BL, et al. The yeast lgl family member Sro7p is an effector of the secretory Rab GTPase Sec4p. *J Cell Biol.* 2006;172(1):55–66.
73. Hattendorf DA, Andreeva A, Gangar A, Brennwald PJ, Weis WI. Structure of the yeast polarity protein Sro7 reveals a SNARE regulatory mechanism. *Nature*. 2007;446(7135):567–571.
74. Schwab Y, Mouton J, Chasserot-Golaz S, Marty I, Maulet Y, Jover E. Calcium-dependent translocation of synaptotagmin to the plasma membrane in the dendrites of developing neurones. *Mol Brain Res*. 2001;96(1–2):1–13.
75. Tang J, Maximov A, Shin OH, Dai H, Rizo J, Sudhof TC. A complexin/synaptotagmin 1 switch controls fast synaptic vesicle exocytosis. *Cell.* 2006;126(6):1175–1187.
76. Seven AB, Brewer KD, Shi L, Jiang QX, Rizo J. Prevalent mechanism of membrane bridging by synaptotagmin-1. *Proc Natl Acad Sci U S A*. 2013;110(34):E3243–E3E52.
77. Xu JJ, Brewer KD, Perez-Castillejos R, Rizo J. Subtle Interplay between synaptotagmin and complexin binding to the SNARE complex. *J Mol Biol.* 2013;425(18):3461–3475.
78. Blagoveshchenskaya AD, Hannah MJ, Allen S, Cutler DF. Selective and signal-dependent recruitment of membrane proteins to secretory granules formed by heterologously expressed von Willebrand factor. *Mol Biol Cell.* 2002;13(5):1582–1593.
79. Giblin JP, Hewlett LJ, Hannah MJ. Basal secretion of von Willebrand factor from human endothelial cells. *Blood*. 2008;112(4):957–964.
80. Cheviet S, et al. Tomosyn-1 is involved in a post-docking event required for pancreatic β-cell exocytosis. *J Cell Sci*. 2006;119(pt 14):2912–2920.
81. Kanaji S, Fahs SA, Shi Q, Haberichter SL, Montgomery RR. Contribution of platelet vs. endothelial VWF to platelet adhesion and hemostasis. *J Thromb Haemost*. 2012;10(8):1646–1652.
82. Morrell CN, Matsushita K, Lowenstein CJ. A novel inhibitor of N-ethylmaleimide-sensitive factor decreases leukocyte trafficking and peritonitis. *J Pharmacol Exp Ther*. 2005;314(1):155–161.
83. Dayananda KM, Gogia S, Neelamegham S. Escherichia coli-derived von Willebrand factor-A2 domain fluorescence/Forster resonance energy transfer proteins that quantify ADAMTS13 activity. *Anal Biochem*. 2011;410(2):206–213.
84. Widberg CH, Bryant NJ, Girotti M, Rea S, James DE. Tomosyn interacts with the t-SNAREs syntaxin4 and SNAP23 and plays a role in insulin-stimulated GLUT4 translocation. *J Biol Chem.* 2003;278(37):35093–35101.
85. Morrell CN, et al. Glutamate mediates platelet activation through the AMPA receptor. *J Exp Med*. 2008;205(3):575–584.
86. Owens AP, et al. Towards a standardization of the murine ferric chloride-induced carotid arterial thrombosis model. *J Thromb Haemost*. 2011;9(9):1862–1863.
87. Eckly A, et al. Mechanisms underlying $FeCl_3$-induced arterial thrombosis. *J Thromb Haemost*. 2011;9(4):779–789.